THE JOURNAL OF BIOLOGICAL CHEMISTRY
Vol. 280, No. 35, Issue of September 2, pp. 31249–31256, 2005
Printed in U.S.A.

Crystal Structure of the *Actinomadura* R39 DD-peptidase Reveals New Domains in Penicillin-binding Proteins*

Received for publication, March 24, 2005, and in revised form, June 10, 2005
Published, JBC Papers in Press, June 29, 2005, DOI 10.1074/jbc.M503271200

Eric Sauvage‡, Raphaël Herman, Stephanie Petrella§, Colette Duez¶, Fabrice Bouillenne, Jean-Marie Frère, and Paulette Charlier

From the Centre d'Ingénierie des Protéines, Université de Liège, Institut de Physique B5, B-4000 Liège, Belgium

***Actinomadura* sp. R39 produces an exocellular DD-peptidase/penicillin-binding protein (PBP) whose primary structure is similar to that of *Escherichia coli* PBP4. It is characterized by a high β-lactam-binding activity (second order rate constant for the acylation of the active site serine by benzylpenicillin: k_2/K = 300 $mM^{-1}s^{-1}$). The crystal structure of the DD-peptidase from *Actinomadura* R39 was solved at a resolution of 1.8 Å by single anomalous dispersion at the cobalt resonance wavelength. The structure is composed of three domains: a penicillin-binding domain similar to the penicillin-binding domain of *E. coli* PBP5 and two domains of unknown function. In most multimodular PBPs, additional domains are generally located at the C or N termini of the penicillin-binding domain. In R39, the other two domains are inserted in the penicillin-binding domain, between the S*XX*K and S*X*N motifs, in a manner similar to "Matryoshka dolls." One of these domains is composed of a five-stranded β-sheet with two helices on one side, and the other domain is a double three-stranded β-sheet inserted in the previous domain. Additionally, the 2.4-Å structure of the acyl-enzyme complex of R39 with nitrocefin reveals the absence of active site conformational change upon binding the β-lactams.**

Cell wall assembly is catalyzed by a series of active-site serine DD-peptidases, known as penicillin-binding proteins (PBPs).[1] These enzymes catalyze the final steps in the synthesis of cell wall peptidoglycan, a highly cross-linked mesh that surrounds the bacteria and protects them from osmotic shock and lysis. They constitute the lethal targets of penicillins and more generally of β-lactam antibiotics, which exhibit a rough structural analogy with the PBP peptide substrates, *i.e.* the D-alanyl-D-alanine C termini of peptidoglycan stem peptides. β-Lactams acylate the active site serine of the penicillin-binding domain of PBPs and form a rather stable acyl-enzyme devoid of transpeptidase activity (1).

Multiple PBPs, from three in *Neisseria meningiditis* to twelve in *Escherichia coli*, are bound to the cytoplasmic membrane of all bacteria. These PBPs can be divided into two groups: the high molecular mass PBPs, which are multimodular enzymes containing a DD-transpeptidase domain associated either with a transglycosylase domain or with a domain of unknown function and the low molecular mass PBPs, which act mainly as DD-transpeptidases or DD-carboxypeptidases (2, 3). Low molecular mass PBPs are further divided into classes A, B, and C according to their sequences (1, 4). Structural information on class A and class B low molecular mass PBPs has been made available through crystal structures determination of *E. coli* PBP5 (5) and the *Streptomyces* K15 DD-peptidase (K15) (6), two representatives of the class A, and of the *Streptomyces* R61 DD-transpeptidase-carboxypeptidase (R61) (7), a well studied enzyme representative of class B. The overall fold of PBP5 is that of class A β-lactamases with a C-terminal extension domain, whereas R61 is similar to class C β-lactamases. Despite the absence of crystal structure of class C low molecular mass PBPs, similarities with class A β-lactamases have been highlighted. Compared with the class A β-lactamase structures, these proteins exhibit an additional domain of about 200 residues inserted between the S*XX*K and the S*X*N conserved motifs characteristic of the penicillin-binding domain (8, 9).

The *Actinomadura* sp. strain R39 DD-peptidase (R39) is a class C low molecular mass PBP that is related to *E. coli* PBP4 (8), *Bacillus subtilis* PBP4a (10, 11), and *Neisseria gonorrhoeae* PBP3 (12). The members of this class of PBPs exhibit medium to high sensitivity to β-lactams, DD-carboxypeptidase, and transpeptidase activity. They also exhibit a so-called endopeptidase activity, *i.e.* they can release a C-terminal residue bearing a large and complex side chain, which is in fact a facet of their carboxypeptidase activity. Moreover, in contrast to most other PBPs, which are strongly anchored in the membrane, class C low molecular mass PBPs are soluble or loosely bound to the membrane via an amphiphilic C-terminal helix (10, 13). Under laboratory growth conditions *E. coli* PBP4 appears to be dispensable, and similar results were found for *B. subtilis* PBP4a and *N. gonorrhoeae* PBP3.

In addition to the low molecular mass PBPs, a few high molecular mass PBPs have been crystallized: *Streptococcus*

* This work was supported in part by the Belgian Program on Interuniversity Poles of Attraction initiated by the Belgian State, Prime Minister's Office, Science Policy Programming (Grant PAI P5/33), by the Fonds National de la Recherche Scientifique (Grants IISN 4.4505.00, FRFC 9.45/9.99, FRFC 2.4.508.01.F, FRFC 9.4.538.03.F, and FRFC 2.4.524.03), and by the University of Liège (Fonds spéciaux, Crédit classique, 1999). The costs of publication of this article were defrayed in part by the payment of page charges. This article must therefore be hereby marked "*advertisement*" in accordance with 18 U.S.C. Section 1734 solely to indicate this fact.

This paper is dedicated to the memory of J.-M. Ghuysen who initiated the study of R39 more than thirty years ago.

The atomic coordinates and structure factors (code 1W79, 1W8Q, and 1W8Y) have been deposited in the Protein Data Bank, Research Collaboratory for Structural Bioinformatics, Rutgers University, New Brunswick, NJ (http://www.rcsb.org/).

‡ To whom correspondence should be addressed: Tel.: 32-43-66-36-20; Fax: 32-43-66-33-64; E-mail: eric.sauvage@ulg.ac.be.

§ A fellow of the French Fondation Recherche Médicale.

¶ Chercheur Qualifié of the Fonds National de la Recherche Scientifique (Brussels, Belgium).

[1] The abbreviations used are: PBP, penicillin-binding protein; K15, *Streptomyces K15* DD-peptidase; R61, *Streptomyces* R61 DD-transpeptidase-carboxypeptidase; R39, *Actinomadura* sp. strain R39 DD-peptidase; PBP5fm, *E. faecium* PBP5; SaG, *Streptomyces* albus G class A β-lactamase; ESRF, European Synchrotron Radiation Facility; SAD, single anomalous diffraction.

TABLE I
Data collection, phasing and refinement statistics

Data set	Co^{2+}	Native	Nitrocefin-soaked
PDB code	1W8Q	1W79	1W8Y
Wavelength (Å)	1.605	0.9763	0.970
Resolution range (Å)[a]	50–2.85 (3.0–2.85)	50–1.8 (1.91–1.8)	50–2.4 (2.55–2.4)
Unique reflections	47,856	187,527	69,694
Redundancy[a]	13.3 (5.5)	3.6 (3.6)	2.9 (2.53)
Completeness (%)[a]	98.0 (86.7)	98.5 (95.6)	86.6 (80.5)
I/σ (I)[a]	20.7 (2.7)	11.7 (3.9)	9.5 (2.2)
R_{sym} (%)[a]	15.3 (71)	9.7 (46)	10.1 (54)
Refinement			
Resolution range (Å)	20–2.85	20–1.8	20–2.4
σ Cutoff	2	2	2
R_{cryst}/R_{free} (%)	19.7/24.4	21.4/24.0	22.7/28.6
Number of protein atoms	13394	13,394	13,394
Number of ions	18 Co^{2+}	4 Mg^{2+}	4 Mg^{2+}
Number of water molecules	80	1781	829
Average B-factors (Å^2)			
Protein	41.9	22.0	43.5
Nitrocefin		40.0	
Water	52.5	34.3	45.3
Root mean square deviations			
Bond lengths (Å)	0.006	0.005	0.007
Bond angles (°)	1.2	1.3	1.3

[a] Statistics for the highest resolution shell are given in parentheses.

pneumoniae PBP2x (14), *Staphylococcus aureus* PBP2a (15), and *Enterococcus faecium* PBP5 (PBP5fm) (16), three class B high molecular mass PBPs involved in determining the level of resistance to β-lactam encountered in these bacteria. The crystal structure of R39 is the first structure of a class C low molecular mass PBP and reveals special structural features that characterize this class of PBPs.

EXPERIMENTAL PROCEDURES

Purification and Crystallization—R39 has been expressed and purified as described previously (8). Crystals were grown at 20 °C by hanging drop vapor diffusion. Native crystals were obtained by mixing 2.5 μl of 25 mg ml^{-1} protein solution (containing 5 mM $MgCl_2$ and 0.1 M Tris) and 2.5 μl of well solution per drop (containing 1.5 M ammonium sulfate and 0.1 M Tris, pH 8). The crystallization conditions were optimized by a search around these conditions and by testing several additives, including different chloride salts. Crystals of the Co^{2+} derivative were prepared by mixing 2.5 μl of 25 mg ml^{-1} protein solution (containing 5 mM $MgCl_2$ and 0.02 M Tris), 2 μl of well solution (containing 2.0 M ammonium sulfate and 0.1 M MES, pH 6), and 0.5 μl of 0.1 M $CoCl_2$ solution. Nitrocefin-soaked crystal were prepared using the same conditions and then transferred to 2 μl of well solution containing nitrocefin (1 mM) for 14 h. Before data collection, crystals were cryoprotected with 100% glycerol.

Data Collection, Phase Determination, and Structure Refinement—Native data were collected at 100 K on an ADSC Quantum 4R charge-coupled device detector at beamline ID29 at the European Synchrotron Radiation Facility (ESRF, Grenoble, France). SAD data and nitrocefin-soaked crystal data were collected at 100 K on a MAR charge-coupled device detector at beamline BM30a at ESRF. All data were processed and scaled using Mosflm (17) and CCP4 (18). The structure was solved by a SAD experiment at the peak wavelength of Co^{2+} K-edge (1.605 Å). The eighteen Co^{2+} sites were found with Solve (19). Phasing with Resolve (20) produced a clearly interpretable electron density map, from which a complete model could be built using Turbo-Frodo (21). This monomer was used as a search model for molecular replacement, with native data. The four monomers in the asymmetric unit were found using AMoRe (22). Subsequent refinement was carried out using CNS (23), and manual model fitting was done with Turbo-Frodo. The four monomers were refined individually. The figures were prepared with Molscript (24), Bobscript (25), and Raster3D (26).

RESULTS

Structure Determination—R39 is a soluble 538-amino acid protein, as deduced from DNA sequence analysis, including a 49-amino acid signal peptide. The tracing of the resulting 489-amino acid R39 molecule in the electron density maps showed that the 23-amino acid C-terminal peptide (467–489) is missing. Subsequent mass spectrometry analyses indicated that the purified enzyme contained 466 residues prior to crystallization.

Because a production system of R39 in *E. coli* was not available and selenomethionine-substituted protein could not be obtained, a search for the presence of anomalous scattering ions, firstly added to enhance crystal growth, was monitored by using a fluorescence detector available at the BM30a beamline at ESRF. A strong fluorescence peak was observed with a crystal grown in presence of Co^{2+}. Thus the use of Co^{2+} ions in the crystallization conditions facilitated the structure determination by single anomalous diffraction at the cobalt resonance wavelength (Table I). R39 crystallizes in space group $P2_1$ (a = 104.56 Å; b = 94.37 Å; c = 106.96 Å; β = 94.05°) with four molecules and eighteen Co^{2+} ions in the asymmetric unit (Fig. 1*A*). The crystallographic environment is similar for molecules A and D and molecules B and C but is different for both pairs. Five Co^{2+} ions are found in molecules A and D, whereas only four are found in molecules B and C. Each Co^{2+} ion is ligated by at least one histidine and one aspartic or glutamic acid residues. In molecule A, a Co^{2+} ion is located between His^{282} and Glu^{466} of a crystallographic symmetry-related molecule of molecule A. The same situation arises for molecule D. Because the crystallographic environment is different for molecules B and C, the absence of cobalt near residue 466 results in a disordered 464–466 segment with elevated temperature factors for residues 464 and 465 and loss of interpretable density for residue 466. The root mean square deviation between any two molecules of the asymmetric unit is between 0.35 and 0.40 Å. The final structure has been refined at 1.8 Å against data collected from a crystal grown in slightly different conditions in the absence of Co^{2+}. In this refined structure, four Mg^{2+} ions are present in the asymmetric unit in sites of four of the 18 Co^{2+} ions. Two of these Mg^{2+} ions are found in molecule A and two in molecule D.

Overall Structure—Topologically, R39 is composed of three distinct domains. The penicillin-binding domain consists of residues 1–65 and 285–466 (Fig. 1, *B* and *C*). The second domain (domain II) comprises residues 66–165 and 237–284 and corresponds to an insertion at the beginning of helix α4 between the motifs S*XX*K and S*X*N, two usual motifs of the PBPs active site. The third domain (domain III) is a subdomain

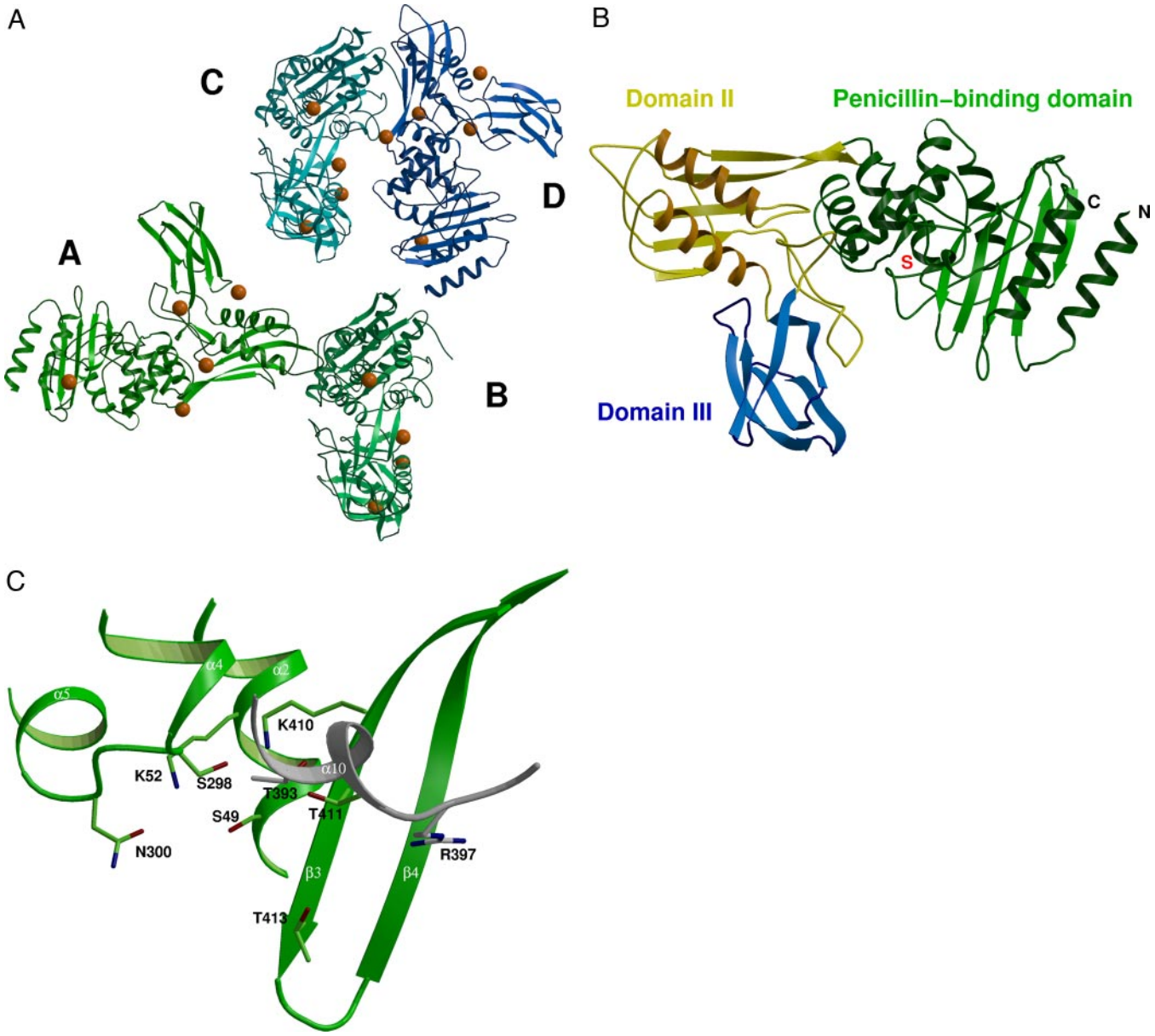

FIG. 1. **Structure of R39.** *A*, asymmetric unit cell representation. Co^{2+} ions are shown as *small brown spheres*. Crystallographic environment is similar for molecules *A* and *D* and molecules *B* and *C* but different for both pairs; *B*, overall structure of R39 shown as a *ribbon diagram*. The penicillin-binding domain is *green*, domain II is *yellow* and *brown*, and domain III is *blue*. The position of the active site serine is indicated by a *red* '*S*'; *C*, active site of R39. Secondary structure elements of the penicillin-binding domain have been labeled in accordance with the labeling scheme of class A β-lactamases. Ser^{49} and Lys^{52} form the first motif S*X*XK characteristic of the penicillin-binding proteins active site. Ser^{298} and Asn^{300} form the second motif S*X*N, and the third motif, KTGT, consists of Lys^{410}, Thr^{411}, Gly^{412}, and Thr^{413}.

inserted in domain II and consists of residues 166–236. Each domain possesses a β-sheet that is oriented approximately at right angle from the β-sheets of the other two domains.

Penicillin-binding Domain—The penicillin-binding domain shares its overall fold with other penicillin-binding proteins and the serine β-lactamases: the R39 active site is located in an extended groove between a five-stranded anti-parallel β-sheet and a cluster of α-helices. The root mean square deviations with the corresponding domains of other PBPs range between 2.2 and 2.8 Å (Table II). Structure-based alignments of these domains reveal significant structural differences. The structures providing the greatest degree of folding similarity are those of *E. coli* PBP5 and class A β-lactamases, with some major differences. The first difference is the replacement of the β-lactamase variable loop inserted before helix α4 by the 220-amino acid peptide corresponding to domains II and III. A loop of R39 domain II extends near the active site, reminiscent of the variable loop in β-lactamases, but the two loops are structurally different. The second difference is the absence of the β-lactamase Ω-like loop defining the bottom of the active site. In this region, the 343–353 segment is folded like its counterpart in PBP5. The third difference is the conformation of the residues surrounding helix α10 in a region situated above the active site (residues 381–408).

TABLE II
Root mean square deviations between the R39 penicillin-binding domain and the corresponding domains of other PBPs

Enzyme	K15	PBP5	R61
Root mean square deviation (Å)	2.23	2.32	2.84
Number of aligned Cα atoms	187	185	192

The residues involved in the enzymatic activity and defining the active site correspond to the three conserved motifs found in

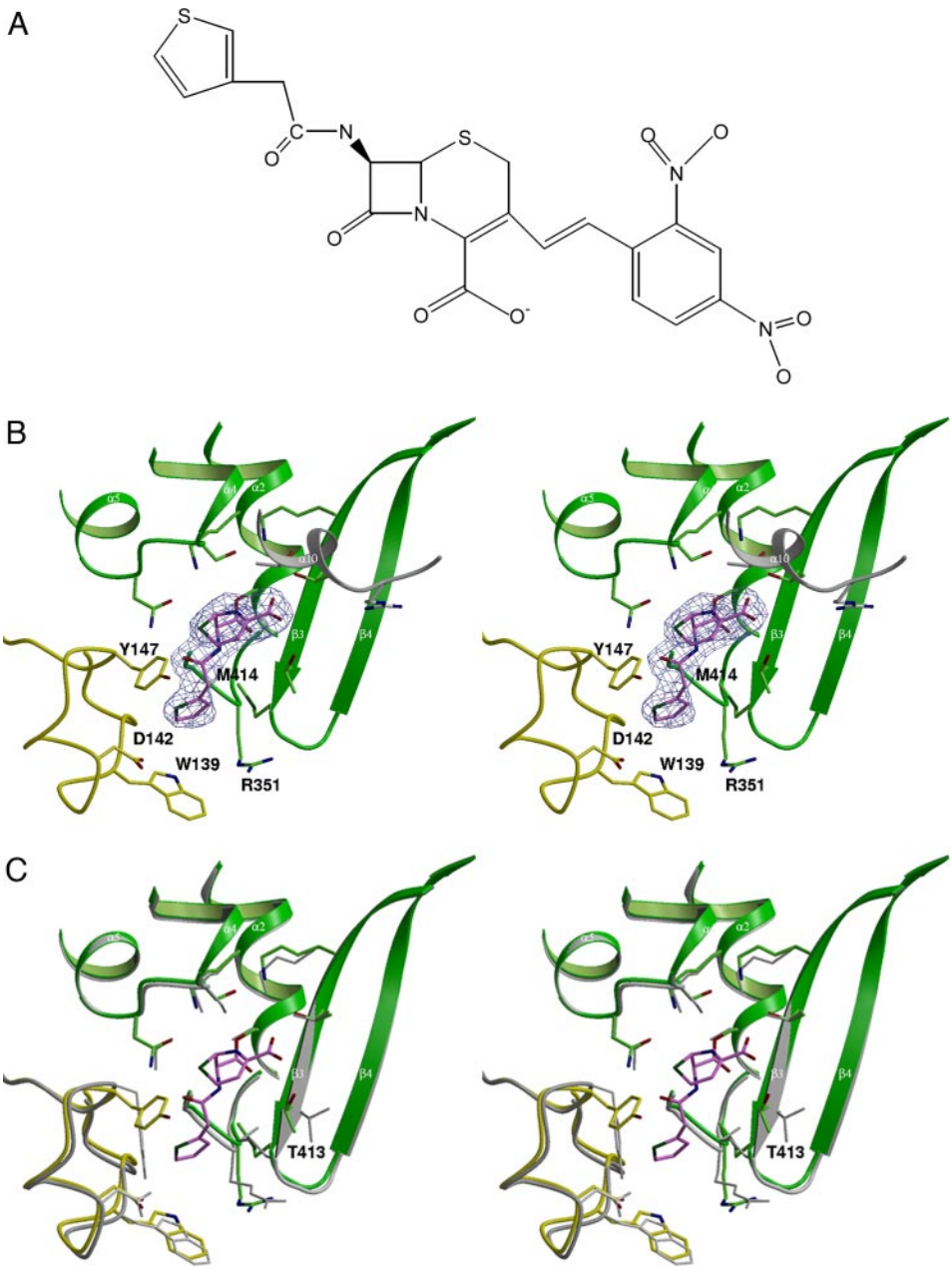

FIG. 2. **Interaction between R39 and nitrocefin.** *A*, structure of nitrocefin; *B*, nitrocefin-R39 acyl-enzyme structure. Stereo view of a $F_{obs} - F_{calc}$ electron density omit map calculated without the nitrocefin molecule, contoured at 2σ. Nitrocefin is *magenta*, the penicillin-binding domain is *green*, and domain II is *yellow*. The side chain of nitrocefin fills a pocket formed by Trp^{139}, Asp^{142}, Tyr^{147}, Arg^{351}, and Met^{414}; *C*, comparison between the structures of the R39 apo-enzyme and the nitrocefin acyl-enzyme. Apo-enzyme is *gray*, and nitrocefin acyl-enzyme is colored as in *B*.

PBPs and class A β-lactamases: Ser^{49}-Xaa-Xaa-Lys^{52} (motif 1), Ser^{298}-Xaa-Asn^{300} (motif 2), and Lys^{410}-Thr^{411}-Gly^{412}-Thr^{413} (motif 3). As in other PBPs, a dense hydrogen bond network prevails in the R39 active site, with a water molecule in the oxyanion hole formed by the backbone nitrogens of Ser^{49} and Thr^{413}. In the upper region of the active site, although the superposition of most PBP backbones does not fit in the surroundings of helix α10, a threonine is frequently observed at the exact position of Thr^{393} (Thr^{199} in K15, Thr^{526} in PBP2x, Thr^{526} in PBP2a, Thr^{603} in PBP5fm, and Thr^{216} in the *Streptomyces albus G* class A β-lactamase (SaG) (27)). Thr^{393} Oδ is hydrogen-bonded to Thr^{411} Oδ and contributes to the hydrogen bond network that strengthens the active site. A distinctive feature of R39 is a specific pocket observed in the bottom of the active site and mainly defined by residues Trp^{139}, Asp^{142}, Tyr^{147}, three residues belonging to domain II, and Arg^{351} and Met^{414}, two residues of the penicillin-binding domain. This characteristic could prove useful in the development of specific β-lactam antibiotics with a high affinity for R39, as developed for the R61 DD-peptidase (28).

Acylation with β-Lactams—R39 is highly sensitive to β-lactams (k_2/K = 2600 mM^{-1} s^{-1} for nitrocefin), and deacylation occurs at a very low rate ($k_3 = 1.5 \times 10^{-6}$ s^{-1}) (3), a favorable situation for the accumulation of an acyl-enzyme. After soaking in nitrocefin, the four molecules present in the asymmetric unit are acylated. The electron density of the R39 active site unambiguously reveals a covalent acyl-enzyme with nitrocefin (Fig. 2). The dihydrothiazolidine ring and the carboxylate are well defined, and the electron density is continuous between the active site serine hydroxyl group and the β-lactam carbonyl group. There is no density for the R2 substituent of nitrocefin. Departure of the C3′ substituent after electronic rearrangement upon opening of the β-lactam ring has been observed in acyl-enzyme complexes of R61 and PBP2x with cephalosporins (29, 30), but not in the acyl-nitrocefin-PBP2a structure (15). Apart from the

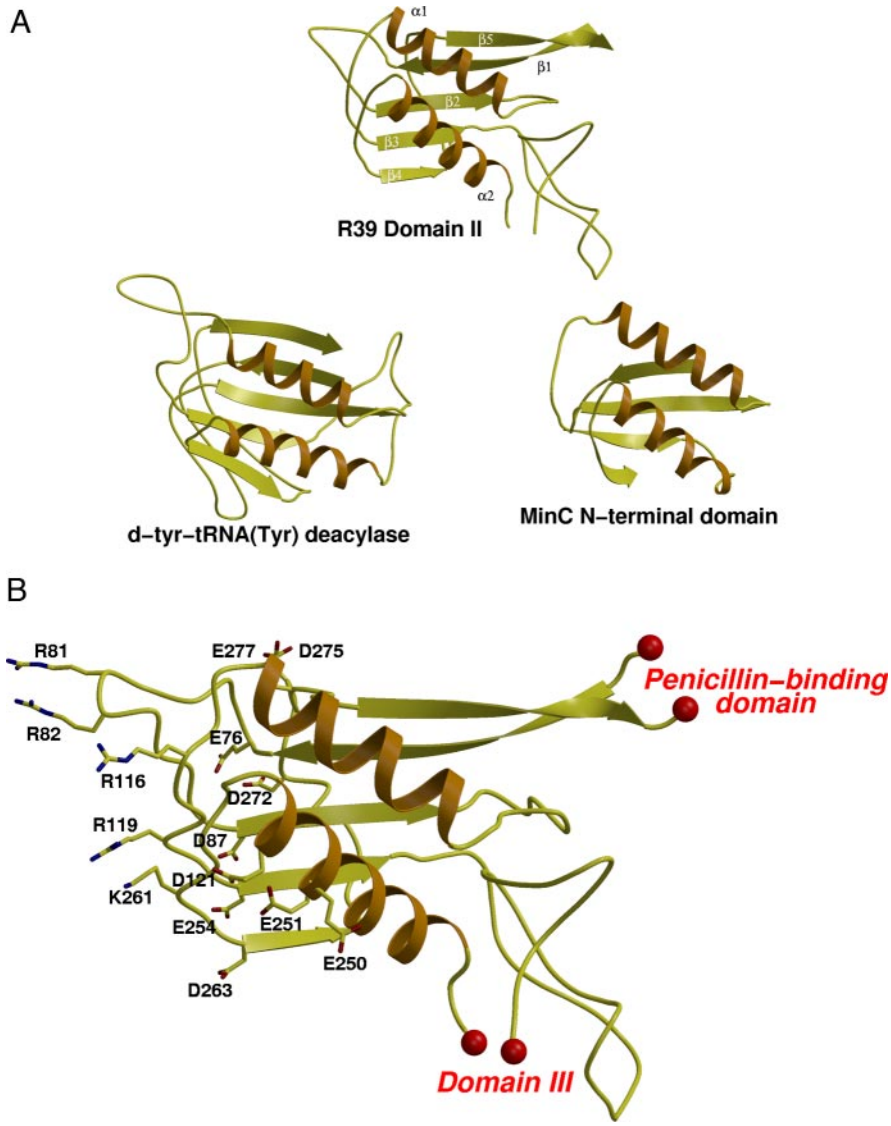

FIG. 3. **Structure of R39 domain II.** *A*, structural comparison of R39 domain II, *d*-Tyr-tRNA deacylase, and the N-terminal domain of MinC. Secondary structures of domain II are labeled; *B*, dipolar head of R39 domain II. Nitrogen atoms are colored *blue*; oxygen atoms are colored *red*. Connections with the penicillin-binding domain and domain III are represented by *small red spheres*.

R2 substituent, the position of nitrocefin in the active site is similar to that observed with PPB2a. The amide group in the nitrocefin side-chain hydrogen bonds to Asn^{300} Oδ1 and to the backbone carbonyl of Thr^{413}, the β-lactam carbonyl oxygen being located in the oxyanion hole. The nitrocefin carboxylate is hydrogen bonded to Thr^{411} and Thr^{413}, as observed in many acyl-PBPs complexes. It is noteworthy that, among 25 class C low molecular mass PBPs sequences aligned with R39 in a Blast search (31), Arg^{397} is one of the few strictly conserved residues. Its position in helix α10 is equivalent to the position of Arg^{220} in SaG. Owing to the α10 position, which is slightly different in class A β-lactamases and R39, the distance between the guanidinium group and the β-lactam carboxylate is 6.2 Å, whereas a direct interaction between these two groups is generally observed in acyl-enzyme intermediates of class A β-lactamases.

The R39 active site does not undergo a great structural deformation upon β-lactam binding. The main effect of acylation on the R39 structure is a slight tilt of the β3 strand and a displacement of Thr^{413} (Fig. 2*C*). The side chain of Thr^{413} moves 2.35 Å in direction of nitrocefin, allowing for hydrogen bond formation between the substrate carboxylate and the hydroxyl groups of Thr^{411} and Thr^{413}. The situation is identical in all molecules except a slight difference in the position of the nitrocefin C6 substituent and a consequent adaptation of the side chain of residues Tyr^{147} and Met^{414}.

Non Penicillin-binding Domains—Domain II (residues 66–165 and 237–284) is a five-stranded β-sheet with two helices packed on one side (Fig. 3*A*). The sheet is composed of one antiparallel and four parallel strands in the order $\beta5_{II}$-$\beta1_{II}$-$\beta2_{II}$-$\beta3_{II}$-$\beta4_{II}$ with $\beta1_{II}$ anti-parallel. Strand $\beta2_{II}$ is followed by helix $\alpha1_{II}$, and strand $\beta3_{II}$ is followed by helix $\alpha2_{II}$. The topology as well as the three-dimensional arrangement of the subdomain formed by $\beta2_{II}$-$\alpha1_{II}$-$\beta3_{II}$-$\alpha2_{II}$-$\beta4_{II}$ corresponds to one-half of a Rossmann fold. Using a three-dimensional DALI search (32) with residues 66–165 and 237–284, domain II was found to topologically resemble domains of *E. coli* d-Tyr-$tRNA^{Tyr}$ deacylase (33) (PDB 1JKE) and barley 1,3–1,4-β-glucanase (34) (PDB 1AQ0) with Z-scores of 5.5 and 4.7, respectively. Indeed, the five strands and the two helices can be superimposed with a root mean square value of 3.1 Å for 82 aligned Cα atoms for the d-Tyr-$tRNA^{Tyr}$ deacylase and 3.5 Å for 74 aligned Cα atoms for the 1,3–1,4-β-glucanase. Domain II is also topologically similar to the N-terminal domain of MinC (35) and the 1A region of FtsA (36), two proteins interacting with FtsZ and involved in the regulation of the septum formation in cell division. However the resemblance between R39 and both MinC and FtsA remains limited. Moreover, R39 lacks sequence homology with all these topologically similar proteins and the loops connecting the secondary structures are completely different.

A β hairpin connects strands $\beta1_{II}$ and $\beta2_{II}$. Two arginines

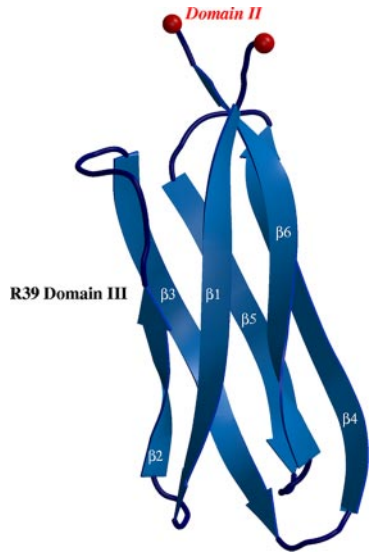

FIG. 4. **Structure of R39 domain III.** The six β-strands of domain III are labeled. Connections with domain II are represented by *small red spheres*.

(Arg^{81} and Arg^{82}) constitute the head of the hairpin with their side chain protruding out of the core of domain II. Similarly, the side chains of Arg^{116} and Arg^{119}, located in the loop connecting $\alpha 1_{II}$ and $\beta 3_{II}$, extend on the same side of domain II. These four arginines, together with Lys^{261}, form a positively charged surface on the side opposite to the interface with the penicillin-binding domain. The side chains of these residues seem to float into the solvent. Accordingly, the temperature factors of the side chains are high, and the electron density around them is quite poor. A crown of negatively charged residues (Glu^{76}, Asp^{87}, Asp^{121}, Glu^{250}, Glu^{251}, Glu^{254}, Asp^{263}, Asp^{272}, Asp^{275}, and Glu^{277}) surrounds this positively charged head (Fig. 3*B*). This dipolar surface might be involved in protein-protein interaction. On the opposite side, following $\beta 3_{II}$ strand, a long unstructured loop (126–153) extends out of domain II. It packs onto the penicillin-binding domain, with residues Trp^{139}, Asp^{142}, and Tyr^{147} being part of a specific pocket in the bottom of the active site. A small β hairpin connects this loop to domain III.

Domain III consists of two three-stranded β-sheets facing each other in a kind of incomplete β-barrel (Fig. 4). The first β-sheet is an antiparallel β-sheet made of strands $\beta 2_{III}$-$\beta 1_{III}$-$\beta 6_{III}$. The second β-sheet consists of strands $\beta 3_{III}$-$\beta 5_{III}$-$\beta 4_{III}$, $\beta 5_{III}$ being parallel to $\beta 3_{III}$ and antiparallel to $\beta 4_{III}$. A DALI search with residues 166–236 did not yield any structurally similar protein (Z smaller than 2.5 and no equivalence with visual inspection).

DISCUSSION

The *Actinomadura* R39 DD-peptidase is encoded by a 1614-nucleotide gene. The 538-amino acid protein precursor presents a 49-amino acid N-terminal signal peptide and, presumably, a 23-amino acid C-terminal extension that are both cleaved to yield a mature soluble protein of 466 residues. When the protein is produced in *Streptomyces lividans* TK24 grown in YEME (Difco yeast extract, 3 g; Difco bactopeptone, 5 g; Oxoid malt extract, 3 g; glucose, 10 g; sucrose, 340 g) medium, its molecular mass is about 3 kDa higher than the molecular mass exhibited by the protein purified from the culture supernatant of *Actinomadura* R39. Moreover, the protein produced in *S. lividans* lacks both DD-peptidase activity and penicillin-binding ability. The mass difference associated with loss of enzymatic activity was first thought to be an incorrect processing of the signal peptide (8), but it might also result from an incorrect processing of the C-terminal extension. A similar situation has been observed with the R61 DD-peptidase, for which the precursor containing the C-terminal extension was shown to be inactive (37). Proteolytic cleavage of a C-terminal fragment has been observed in few other cases, although not necessarily associated with enzymatic activity (38–40). Inspection of the R39 three-dimensional structure reveals that the C-terminal extension might reduce the active site accessibility to peptide substrates or β-lactam antibiotics, which would result in a loss of enzymatic activity and β-lactam binding ability.

The mechanism of interaction between PBPs and β-lactam antibiotics is known to follow a three-step pathway involving the rapid reversible formation of a non-convalent Henri-Michaelis complex followed by formation of a long-lived acyl-enzyme intermediate. Evidence supporting this mechanism is given by the crystallographic structure of a non-covalent PBP-β-lactam complex described recently (28) and those of acyl-PBP intermediates that have been solved with different PBPs (15, 16, 28–30). The possible acylation mechanism involved in R39 might be a general base-assisted catalytic process where the role of the general base could be played by an unprotonated lysine (Lys^{52} in R39), a residue strictly conserved in all PBPs. Lys^{52} would abstract a proton from the active serine hydroxyl group to promote the nucleophilic attack on the β-lactam carbonyl by the activated serine Oγ. The proton would subsequently be back donated by Lys^{52} to the β-lactam nitrogen via Ser^{298}. The distances between Ser^{49} Oγ and Lys^{52} Nζ and between Lys^{52} Nζ and Ser^{298} Oγ are, respectively, 2.8 and 2.98 Å, in agreement with this interpretation. In this case, the unprotonated state of Lys^{52} can be promoted by the active site environment and more precisely by the presence of Lys^{410}. An alternative interpretation of the acylation mechanism relies upon a concerted one-step process where the covalent bond formation between the β-lactam and the active serine Ser^{49} is concomitant with the transfer of the Ser^{49} proton directly to Ser^{298} and to the transfer of the Ser^{298} hydroxyl proton to the β-lactam nitrogen (41). Charges on both Lys^{52} and Lys^{410} support the correct orientation of the Ser^{298} hydroxyl group. This explanation could prevail for all penicilloyl serine transferases, including enzymes possessing a tyrosine residue instead of a serine in the second conserved active site motif, such as the R61 DD-peptidase.

Compared with most other PBPs, R39 exhibits a very high β-lactam binding activity. The value of the second order acylation rate constant on benzylpenicillin is 300 mM^{-1} s^{-1} (*i.e.* the highest value to date for a DD-peptidase) and the high k_2/K values obtained for other penicillins and cephalosporins explains the broad spectrum specificity profile of the R39 enzyme (see Ref. 3 for detailed kinetic data on R39). Like class A β-lactamases and other low molecular mass PBPs (PBP5 and K15), R39 presents a open active site capable of accommodating most β-lactam antibiotics. Many factors may impair the ability of a PBP to bind β-lactams. For example, in the highly resistant *Staphylococcus aureus* PBP2a, there is a narrow binding cavity (the distance between Asn^{300} Oδ1 and Thr^{413} backbone nitrogen is 9 Å in R39, whereas this distance is 6.7 Å in the apo structure of PBP2a). As a result, this cavity must be enlarged to accommodate the incoming antibiotic and the active site needs undergoing conformational changes at strand β3 and at the helix α2 N terminus for acylation to occur (15). Modification of active site catalytic residues may also reduce acylation rate constants. In K15, the enzyme has a very poor β-lactam binding activity, because a cysteine, instead of an asparagine, is present at the position equivalent to Asn^{300} (6). Nothing prevents an efficient acylation of R39 by β-lactams and if R39 is the best

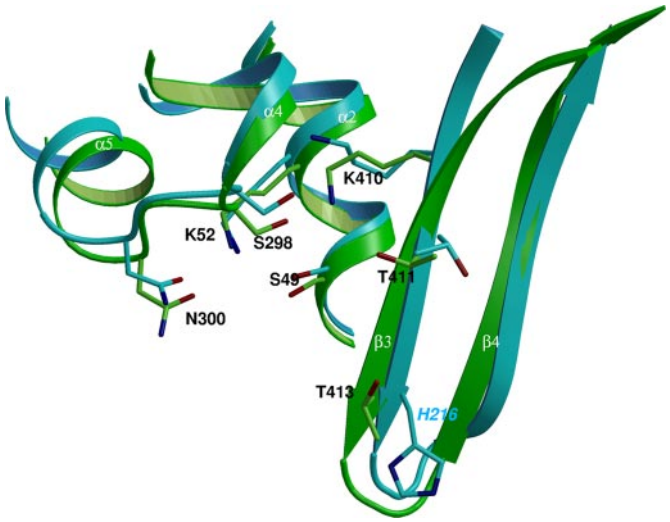

FIG. 5. **Comparison between structures of R39 and *E. coli* PBP5.** The penicillin-binding domain of R39 is *green*, and domain II is *yellow*. PBP5 is *cyan*.

β-lactam-binding DD-peptidase, this is due to the fact that the active site of other PBPs are less accessible or lack the complete set of amino acids involved in the acylation machinery.

The R39 active site structure is very similar to that of PBP5 (Fig. 5). The main difference that could explain the differences between the β-lactam acylation rates of these two enzymes is the substitution of Thr^{413} by a histidine. Many acyl-PBP complexes are stabilized by a hydrogen bond between this threonine and the substrate carboxylate. The R39 active site is also very similar to that of class A β-lactamases. The similarity of low molecular mass PBPs to class A β-lactamases has been previously pointed out (1, 4), and the presence, near the active site, of Arg^{397}, which is strictly conserved in class C low molecular mass PBPs, suggests that both enzymes might have evolved divergently from the same gene. Indeed, conformational changes in residues surrounding helix α10 may bring Arg^{397} in a position equivalent to Arg^{220} in SaG. It has been shown that this arginine favors acylation of class A β-lactamases by β-lactam antibiotics thanks to a strong interaction between the guanidinium group of arginine and the substrate carboxylate (42). In R39, even if the distance between the guanidinium and the carboxylate is more than 6 Å, Arg^{397} might influence the enzymatic activity, for example by interacting with the C-terminal carboxylate of the peptide substrate, as seen in the structure of the R61 DD-peptidase with its peptide substrate (43). Alternatively, the Arg^{397} guanidinium group might interact with the complex side chain of a meso-diaminopimelic acid residue and thus be linked to the 'endopeptidase' activity of the enzyme. The exact role of this residue can be addressed by site-directed mutagenesis.

The most distinctive feature of the R39 active site is the pocket located in the bottom of the active site and formed by residues Trp^{139}, Asp^{142}, Tyr^{147}, Arg^{351}, and Met^{414}. Trp^{139}, Asp^{142}, and Tyr^{147} belong to domain II, a unique domain only found in class C PBPs. This pocket could be specific to accommodate the N-terminal portion of the diaminopimelic acid component typical of the *Actinomadura* cell wall peptidoglycan. In R61, such a specific subsite, different from the R39 one, has been shown to be responsible for the high affinity of R61 for its cell wall peptidoglycan (43).

As with most PBPs, the deacylation step in R39 is extremely slow compared with the efficiency of the deacylation step in class A β-lactamases (a factor up to 10^8). In the latter a glutamic acid of the Ω-loop defining the bottom of the active site (Glu^{166}) activates a conserved water molecule that attacks the acyl-enzyme carbonyl, resulting in very high deacylation rates. In R39, the 343–353 loop in the bottom of the active site is folded like its counterpart in PBP5 but lacks the conserved Asp^{154} and His^{151} residues that have been hypothesized to be responsible for the relatively high deacylation rate of PBP5 (44). The absence of residue capable of activating a deacylating water molecule as well as the absence of such a deacylating water molecule in the nitrocefin-R39 acyl-enzyme crystal structure would explain the poor deacylation rate of R39.

Low molecular mass PBPs exhibit a high carboxypeptidase activity, but class C low molecular mass PBPs also have an 'endopeptidase' activity that is generally not encountered in other PBPs. Where and when class C low molecular mass PBPs might require one of these enzymatic activities remains unclear, and their physiological role is still unknown. It has been suggested that the endopeptidase activity of *E. coli* PBP4 is involved in breaking peptide cross-links to allow the insertion of new glycan strands into the murein sacculus (45). Recent investigations have assigned a role to this PBP in determining a uniform morphology thanks to the same activity, *i.e.* removal of inappropriate cross-links initiated by PBP5. *In vivo* the enzyme seems to behave as a DD-carboxypeptidase rather than a transpeptidase (46, 47). In *B. subtilis*, it was shown that PBP4a is expressed during the late exponential phase but is dispensable for the synthesis of spore peptidoglycan (10, 48).

The structure of R39, with its two additional non-penicillin binding domains, suggests that R39 and more generally class C PBPs could be part of a proteic complex. The resemblance of the R39 domain II topology with *E. coli* d-Tyr-$tRNA^{Tyr}$ deacylase and barley 1,3–1,4-β-glucanase is astonishing but seems unlikely to be associated with the functional properties of these enzymes. Although *B. subtilis* PBP4a was shown to be absent from the septum site (49), it is interesting that interactions between proteins of the septation machinery and minor peptidoglycan-modifying enzymes have been shown to be responsible for significant aspects of bacterial shape determinations (50). Although very limited, the resemblance of R39 domain II to the N-terminal domain of MinC and the 1A region of FtsA, two proteins involved in the regulation of septum formation, suggests that class C low molecular mass PBPs could interact with a protein of the septation machinery. The interacting partner of domain II, if any, remains to be identified if one is to understand the physiological importance of this element of class C low molecular mass PBPs.

Acknowledgments—We thank the staff of beamlines ID29 and BM30a at ESRF for assistance in data collection and J. A. Kelly for critical reading of the manuscript.

REFERENCES

1. Ghuysen, J. M. (1991) *Annu. Rev. Microbiol.* **45,** 37–67
2. Foster, S. J., and Popham, D. L. (2001) in *Bacillus subtilis and Its Relatives: From Genes to Cells* (Sonenshein, L., Losick, R., and Hoch, J. A., eds) pp. 21–41, American Society for Microbiology Press, Washington, D. C.
3. Frere, J. M., and Joris, B. (1985) *Crit. Rev. Microbiol.* **11,** 299–396
4. Massova, I., and Mobashery, S. (1998) *Antimicrob. Agents Chemother.* **42,** 1–17
5. Nicholas, R. A., Krings, S., Tomberg, J., Nicola, G., and Davies, C. (2003) *J. Biol. Chem.* **278,** 52826–52833
6. Fonze, E., Vermeire, M., Nguyen-Disteche, M., Brasseur, R., and Charlier, P. (1999) *J. Biol. Chem.* **274,** 21853–21860
7. Kelly, J. A., and Kuzin, A. P. (1995) *J. Mol. Biol.* **254,** 223–236
8. Granier, B., Duez, C., Lepage, S., Englebert, S., Dusart, J., Dideberg, O., Van Beeumen, J., Frere, J. M., and Ghuysen, J. M. (1992) *Biochem. J.* **282,** 781–788
9. Mottl, H., Nieland, P., de Kort, G., Wierenga, J. J., and Keck, W. (1992) *J. Bacteriol.* **174,** 3261–3269
10. Pedersen, L. B., Murray, T., Popham, D. L., and Setlow, P. (1998) *J. Bacteriol.* **180,** 4967–4973
11. Duez, C., Vanhove, M., Gallet, X., Bouillenne, F., Docquier, J., Brans, A., and Frere, J. (2001) *J. Bacteriol.* **183,** 1595–1599
12. Stefanova, M. E., Tomberg, J., Olesky, M., Holtje, J. V., Gutheil, W. G., and Nicholas, R. A. (2003) *Biochemistry* **42,** 14614–14625
13. Harris, F., Brandenburg, K., Seydel, U., and Phoenix, D. (2002) *Eur. J. Bio-*

chem. **269,** 5821–5829
14. Pares, S., Mouz, N., Petillot, Y., Hakenbeck, R., and Dideberg, O. (1996) *Nat. Struct. Biol.* **3,** 284–289
15. Lim, D., and Strynadka, N. C. (2002) *Nat. Struct. Biol.* **9,** 870–876
16. Sauvage, E., Kerff, F., Fonze, E., Herman, R., Schoot, B., Marquette, J. P., Taburet, Y., Prevost, D., Dumas, J., Leonard, G., Stefanic, P., Coyette, J., and Charlier, P. (2002) *Cell Mol. Life Sci.* **59,** 1223–1232
17. Leslie, A. G. W. (1991) *Crystallographic Computing* **5,** 50–61
18. CCP4. (1994) *Acta Crystallogr. D Biol. Crystallogr.* **50,** 760–763
19. Terwilliger, T. C., and Berendzen, J. (1999) *Acta Crystallogr. D Biol. Crystallogr.* **55,** 849–861
20. Terwilliger, T. C. (2000) *Acta Crystallogr. D Biol. Crystallogr.* **56,** 965–972
21. Roussel, A., and Cambillau, C. (1989) in *Silicon Graphics Geometry Partner Directory*, Silicon Graphics, Mountain View, CA
22. Navaza, J. (2001) *Acta Crystallogr. D Biol. Crystallogr.* **57,** 1367–1372
23. Brunger, A. T., Adams, P. D., Clore, G. M., DeLano, W. L., Gros, P., Grosse-Kunstleve, R. W., Jiang, J. S., Kuszewski, J., Nilges, M., Pannu, N. S., Read, R. J., Rice, L. M., Simonson, T., and Warren, G. L. (1998) *Acta Crystallogr. D Biol. Crystallogr.* **54,** 905–921
24. Kraulis, P. J. (1991) *J. Appl. Crystallogr.* **24,** 946–950
25. Esnouf, R. M. (1997) *J. Mol. Graph. Model* **15,** 112–113, 132–134
26. Merritt, E. A., and Murphy, M. E. (1994) *Acta Crystallogr. D Biol. Crystallogr.* **50,** 869–873
27. Dideberg, O., Charlier, P., Wery, J. P., Dehottay, P., Dusart, J., Erpicum, T., Frere, J. M., and Ghuysen, J. M. (1987) *Biochem. J.* **245,** 911–913
28. Silvaggi, N. R., Josephine, H. R., Kuzin, A. P., Nagarajan, R., Pratt, R. F., and Kelly, J. A. (2005) *J. Mol. Biol.* **345,** 521–533
29. Kuzin, A. P., Liu, H., Kelly, J. A., and Knox, J. R. (1995) *Biochemistry* **34,** 9532–9540
30. Gordon, E., Mouz, N., Duee, E., and Dideberg, O. (2000) *J. Mol. Biol.* **299,** 477–485
31. Altschul, S. F., Madden, T. L., Schaffer, A. A., Zhang, J., Zhang, Z., Miller, W., and Lipman, D. J. (1997) *Nucleic Acids Res.* **25,** 3389–3402
32. Holm, L., and Sander, C. (1995) *Trends Biochem. Sci.* **20,** 478–480
33. Ferri-Fioni, M. L., Schmitt, E., Soutourina, J., Plateau, P., Mechulam, Y., and Blanquet, S. (2001) *J. Biol. Chem.* **276,** 47285–47290
34. Muller, J. J., Thomsen, K. K., and Heinemann, U. (1998) *J. Biol. Chem.* **273,** 3438–3446
35. Cordell, S. C., Anderson, R. E., and Lowe, J. (2001) *EMBO J.* **20,** 2454–2461
36. Rico, A. I., Garcia-Ovalle, M., Mingorance, J., and Vicente, M. (2004) *Mol. Microbiol.* **53,** 1359–1371
37. Fanuel, L., Granier, B., Wilkin, J. M., Bellefroid-Bourguignon, C., Joris, B., Knowles, J., Komives, E., Van Beeumen, J., Ghuysen, J. M., and Frere, J. M. (1994) *FEBS Lett.* **351,** 49–52
38. Nicolet, Y., Piras, C., Legrand, P., Hatchikian, C. E., and Fontecilla-Camps, J. C. (1999) *Structure Fold Des.* **7,** 13–23
39. Inagaki, N., Yamamoto, Y., and Satoh, K. (2001) *FEBS Lett.* **509,** 197–201
40. Nagasawa, H., Sakagami, Y., Suzuki, A., Suzuki, H., Hara, H., and Hirota, Y. (1989) *J. Bacteriol.* **171,** 5890–5893
41. Dive, G., and Dehareng, D. (1999) *Int. J. Quant. Chem.* **73,** 161–174
42. Jacob-Dubuisson, F., Lamotte-Brasseur, J., Dideberg, O., Joris, B., and Frere, J. M. (1991) *Protein Eng.* **4,** 811–819
43. McDonough, M. A., Anderson, J. W., Silvaggi, N. R., Pratt, R. F., Knox, J. R., and Kelly, J. A. (2002) *J. Mol. Biol.* **322,** 111–122
44. Davies, C., White, S. W., and Nicholas, R. A. (2001) *J. Biol. Chem.* **276,** 616–623
45. Burman, L. G., and Park, J. T. (1984) *Proc. Natl. Acad. Sci. U. S. A.* **81,** 1844–1848
46. Meberg, B. M., Paulson, A. L., Priyadarshini, R., and Young, K. D. (2004) *J. Bacteriol.* **186,** 8326–8336
47. Korat, B., Mottl, H., and Keck, W. (1991) *Mol. Microbiol.* **5,** 675–684
48. Popham, D. L., Gilmore, M. E., and Setlow, P. (1999) *J. Bacteriol.* **181,** 126–132
49. Scheffers, D. J., Jones, L. J., and Errington, J. (2004) *Mol. Microbiol.* **51,** 749–764
50. Varma, A., and Young, K. D. (2004) *J. Bacteriol.* **186,** 6768–6774